

Supplementary Material

Complete Corrosion Inhibition through Graphene Defect Passivation

Ya-Ping Hsieh^{*1}, *Mario Hofmann*², *Kai-Wen Chang*¹, *Jian Gang Jhu*¹, *Yuan-Yao Li*¹, *Kuang Yao Chen*³,
*Chang Chung Yang*³, *Wen-Sheng Chang*³, *Li-Chyong Chen*⁴

¹Graduate Institute of Opto-Mechatronics, National Chung Cheng University, 168 University Road, Min-Hsiung Township, Chiayi County, Taiwan 62102

²Department of Material Science and Engineering, National Cheng Kung University, Tainan, Taiwan 70101

³Green Energy and Environment Research Laboratories, Industrial Technology Research Institute, Hsinchu, Taiwan 31040

⁴Center for Condensed Matter Sciences, National Taiwan University, Taipei, Taiwan 10617

*Address correspondence to yphsieh@ccu.edu.tw

1. Pervasiveness of defects in graphene

We want to emphasize that the graphene employed in this work is of high quality and the presented results reveal an intrinsic behavior of graphene. Optimization of the growth process was carried out to minimize the density of graphene defects. The defectiveness was evaluated by film induced frustrated etching (FIFE)¹ which emulates the corrosion process through exposure of the Cu foil to etchant.

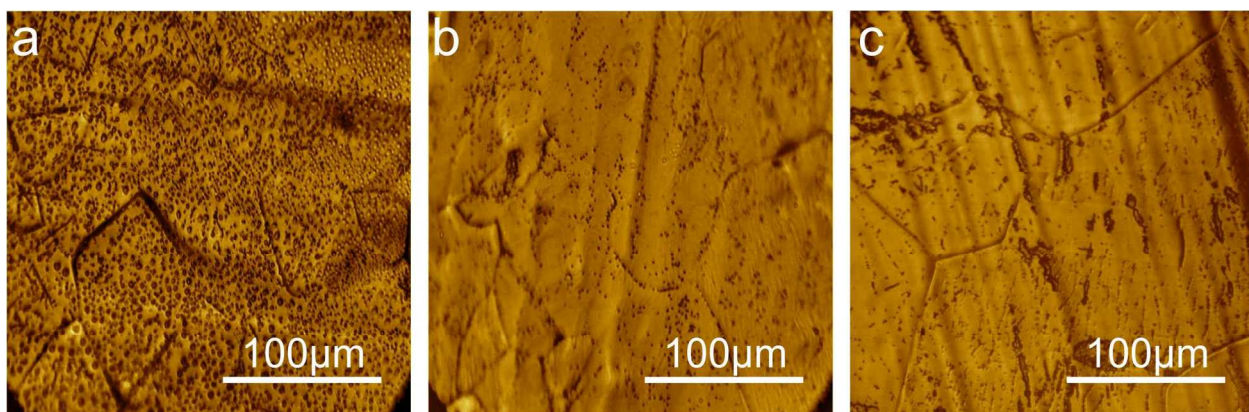


Figure S1. Optical micrographs of Cu/1LG after 10s corrosion: (a) result before growth optimization, (b) result after growth optimization, (c) commercial graphene

To corroborate the high quality of the synthesized graphene we used both Raman spectroscopy and electrical measurements. The ratio of Raman D and G-Band intensity was consistently lower than 5% . Macroscopic Hall effect measurements on square-centimeter samples furthermore reveal an average carrier mobility of $1000\text{cm}^2/\text{Vs}$ which is consistent with high quality CVD graphene.¹ We finally compared our material to commercial graphene samples (Bluestone Global Inc.) and found that the amount of occurring corrosion is similar. These results agree with previous reports that graphene defects are ubiquitous² and future studies will have to reveal strategies to avoid them.³

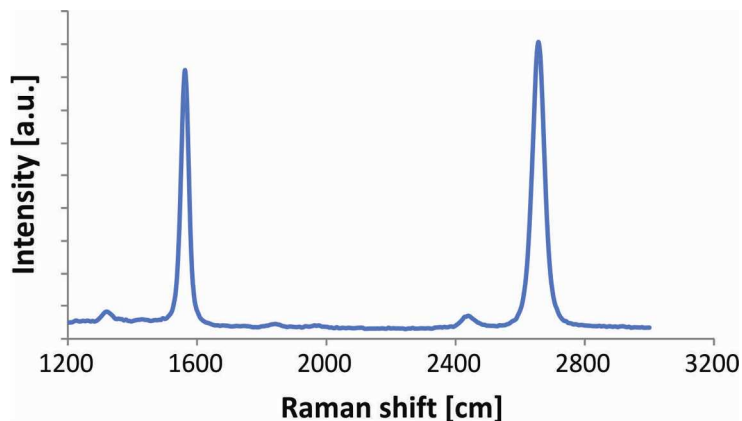


Figure S2. Representative Raman spectrum of Graphene transferred onto SiO₂

2. Measurement of etch speed

Copper foil was annealed and partially protected by Scotch tape. Then, the copper foil was dipped into APS etchant for 5s before immersing it into deionized water and blow drying with Nitrogen. After removing the protecting layer, the step height between the etched and protected Cu was measured by Atomic force microscopy (AFM).

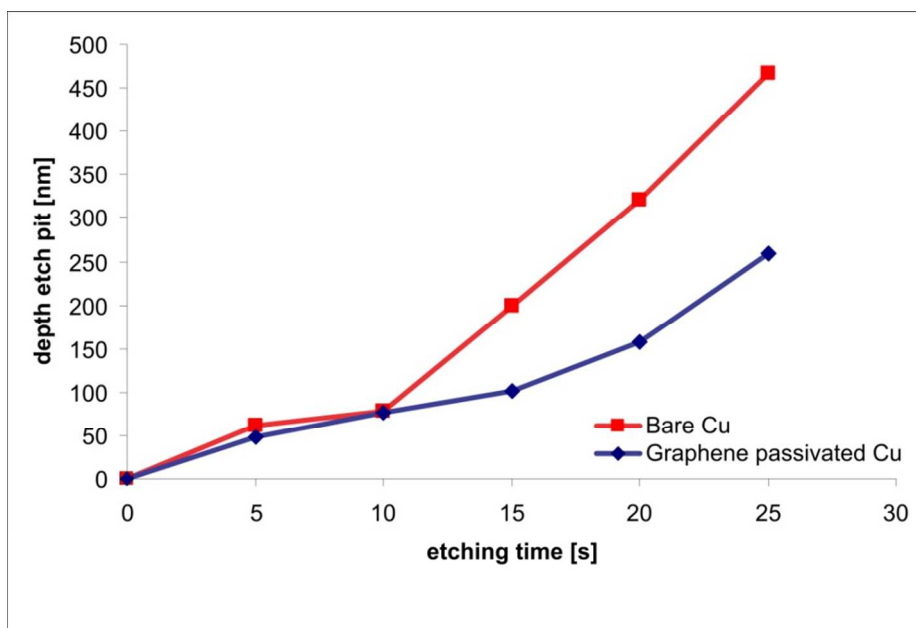


Figure S3. Comparison of etch rates of bare copper substrate and etch pit depth of graphene passivated copper substrate

In addition to determining the exchange rate of molecules through the graphene opening by electrochemical measurements, we attempted to estimate the permeation speed by time resolved analysis of the etching process. We found that etching occurs even when exposing Cu/1LG to etchant for only 0.3s before washing the etchant away. Thus permeation has to occur at a time scale much shorter than 0.3s. Furthermore, from the linear trend of pit dimensions with etching time we infer that the permeation time will remain insignificant compared to the etching time throughout the investigated measurement period of 35s. Consequently, filling the volume of an etch pit even after 35s will proceed at shorter times than 0.3s. Considering the dimension of such an etch pit ($\sim 2.2 \times 0.3 \mu\text{m}$) and an orifice diameter of 1.6nm, the etchant permeation speed through graphene has to be larger than 2.4m/s to fill the etch pit within the given time.

3. Characterization of ALD on Cu and graphene

Atomic layer deposition (ALD) is a sequential chemisorption process that relies on the availability of surface functional groups. Due to the absence of these functional groups on graphene, ALD is expected to result in a different morphology than crystals, such as Cu. Scanning electron microscopy was employed to compare the morphology of ALD on Cu and ALD on graphene. Figure S4 shows significant differences in the morphology after 16nm ALD film deposition. Whereas ALD on Cu seems to form complete films of high roughness, only clusters grow on graphene. The lateral dimension of these clusters upon deposition of 16nm equivalent ALD film thickness are on average ~ 32 nm. This observation suggests that clusters grow out radially from a single seed in agreement with previous reports by Wang *et al.*⁴

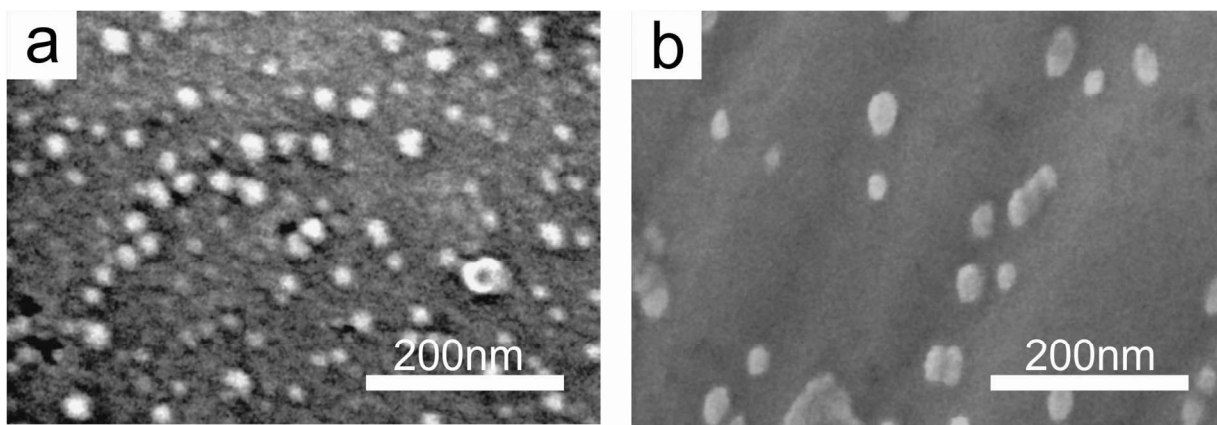


Figure S4. Scanning Electron Microscope images after ALD of 16nm equivalent thickness on (a) bare Cu, (b) Cu/1LG

4. Electrochemical activity of ALD films on Cu and graphene

The difference in sample morphology is expected to have significant impact on their electrochemical behavior. Cyclic voltammetry (CV) measurements were therefore carried out for Cu and Cu/1LG samples with and without ALD. Figure S5 shows the cyclic voltammograms of

the hydrogen reduction peak. This feature will occur at any electrode of sufficient electronic conductance and therefore represents the electrode/electrolyte resistance. The comparison of the spectra for samples with and without ALD, it can be seen that ALD on Cu completely suppresses the hydrogen reduction peak. Cu/1LG samples, on the other hand, show no noticeable decrease of electrochemical activity even after deposition of 16nm ALD.

These results support our hypothesis that ALD does not form continuous films on graphene but passivates defects selectively. From the decrease in peak intensity between Cu/1LG and Cu/1LG/16nm ALD an ALD coverage of 7% was estimated.

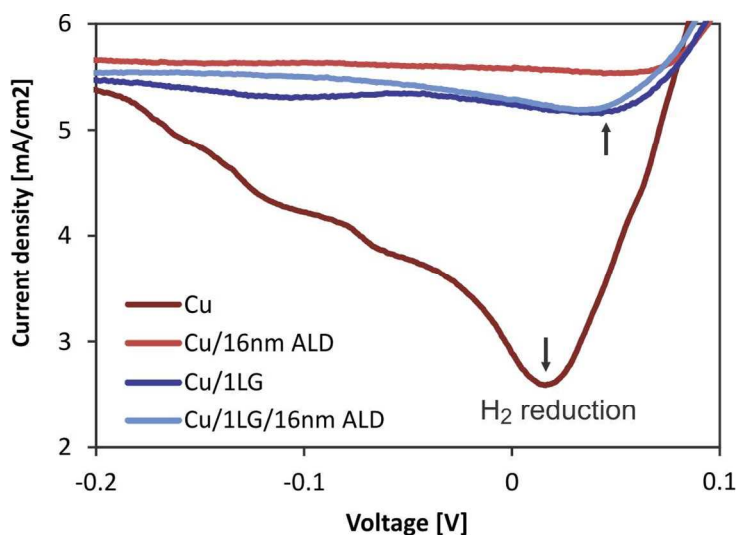


Figure S5. Cyclic voltammograms of hydrogen reduction on Cu and Cu/1LG samples with and without 16nm ALD

5. Tafel analysis

Tafel analysis was carried out under the same conditions as CV. Open circuit potential was measured and its stability was confirmed before sweeping the potential at 5mV/sec.

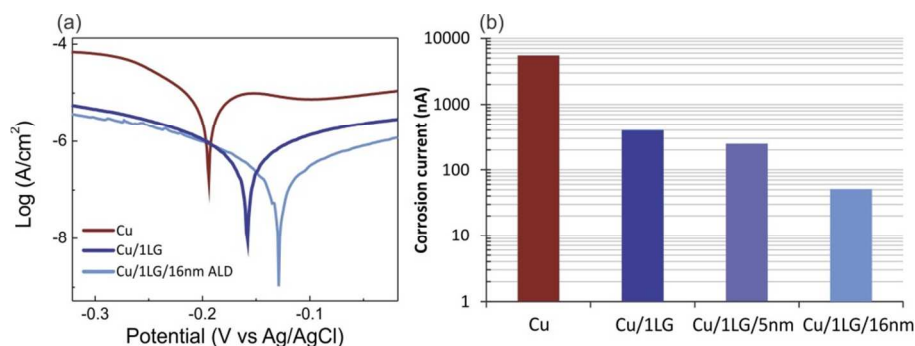


Figure S6. (a) Tafel plot of Cu samples with and without passivation, (b) comparison of corrosion currents on log scale

A clear shift of the intercept between anodic and cathodic branches can be seen for increased passivation which confirms the higher resistance to corrosion. Additionally, the corrosion current is significantly decreased upon passivation by graphene or graphene/ALD. The comparison of bare Cu and Cu/1LG/16nm ALD shows a decrease in corrosion current by 99% which confirms our potentiodynamic measurements. The corrosion rate of Cu/1LG/16nm ALD was found to be $1.6 \times 10^{-15} \frac{m}{s}$ which is comparable to the multilayer graphene on Nickel that was investigated by Prasai *et al.*⁵

The larger passivation efficiency of Cu/1LG compared to our CV results is due to the different source of graphene. For the Tafel measurements graphene grown by atmospheric pressure CVD (APCVD) was used and the occurring larger areas of bilayer graphene provide a better passivation in agreement with reports by Prasai *et al.*⁵ The additional increase of passivation efficiency by 8 times upon ALD, however, indicates that defects exist even in APCVD grown graphene and further passivation is still required.

6. Electrochemical Impedance spectroscopy

Electrochemical impedance spectroscopy (EIS) was carried out under the same conditions as cyclic voltammetry. Representative Bode of bare Cu, graphene and ALD/graphene samples are shown in Figure S7(a,b). The larger impedance values for low frequencies in the Bode plot corroborate that the corrosion resistance of Cu is increased by graphene passivation and can furthermore be improved by ALD passivation of defects. The broadening of the phase angle plot observed for graphene and graphene/ALD samples suggest that this increased passivation is due to the occurrence of two processes with different time constants.

To quantify these observations, equivalent circuit models were constructed. For bare Cu, the contributions of the electrolyte and the electrolyte/metal interface were considered by combining an electrolyte resistance, an interface resistance, and a constant phase element (CPE) (Figure S7(c)). A CPE was used instead of a capacitor because to account for inhomogeneities due to surface oxides on the Cu-foil.⁶ Least-square fitting of EIS spectra obtained for bare Cu finds an interface resistance of $\sim 3\text{k}\Omega$. Upon passivation of the Cu with ALD, the interface resistance increases by 2 orders of magnitude for both 5nm and 16nm equivalent film thickness. This is consistent with our hypothesis that ALD forms a smooth film on the Cu that renders it inert. From these results we can estimate that full coverage of ALD on Cu is reached within the first 50 cycles.

To model the effect of graphene passivation, a pore resistance and a second constant phase element were added to the previous model (Figure S7(d)) following Singh Raman *et al.*⁷ Fitting to this model reveals an increase of the pore resistance by approximately 2 orders of magnitude upon ALD passivation. In contrast to the ALD effect on bare Cu, graphene pore resistance has a direct proportionality with the ALD equivalent film thickness which corroborates our model of selective passivation of defects (Figure S7(d)).

Finally, the graphene pore pseudo-capacitance decreases upon ALD passivation which suggests that the interaction area of the graphene pore is decreased during passivation (Figure S7(d)).

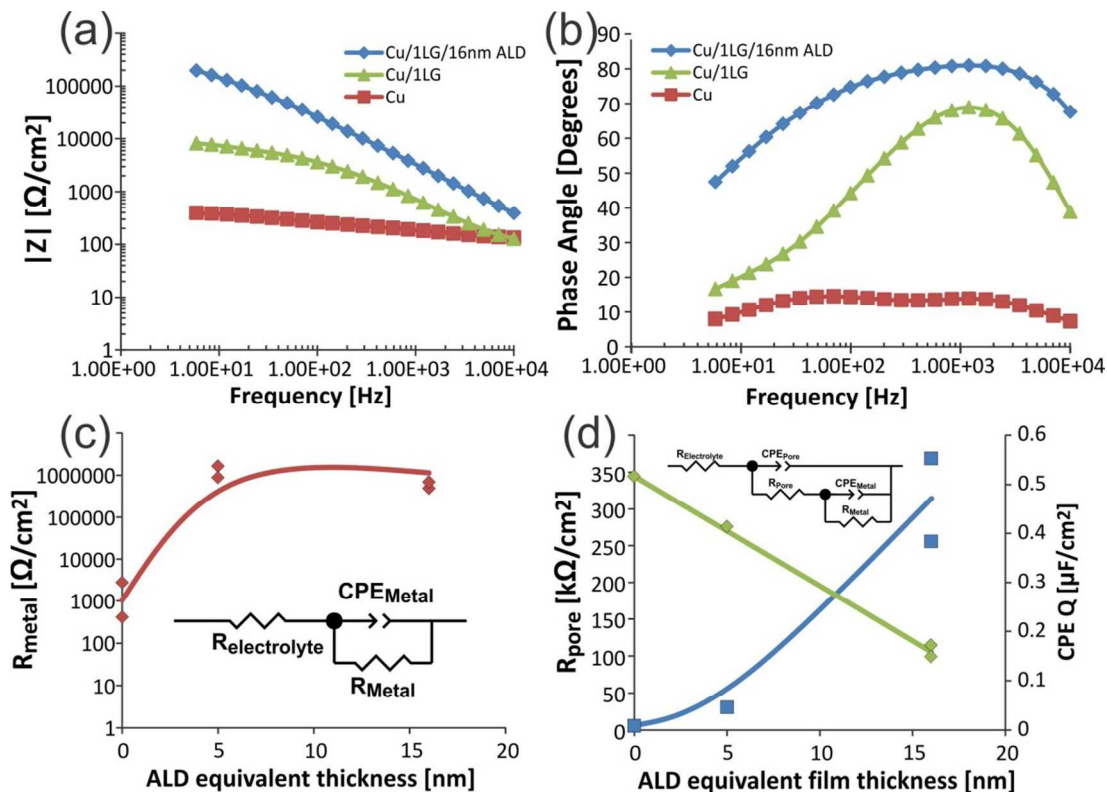


Figure S7. EIS spectroscopy results: Bode plots of impedance (a) and phase angle(b) of Cu samples with and without passivation, (c) Interface resistance of bare Cu upon ALD deposition (inset) equivalent circuit, (d) Pore resistance and pseudocapacitance Q of graphene passivated Cu upon ALD passivation (inset) equivalent circuit.

7. Copper morphology after extended etching

Optical micrographs were taken after 3 hours of electrochemical corrosion tests using continuous CV cycling. The comparison of Cu morphology before etching (Fig. S8) and after etching shows that neither 1LG nor 3LG is sufficient to protect the substrate. The combination of

1LG and 16nm ALD, however, shows very limited etching even after 3hours and confirms the potential of graphene based passivation methods.

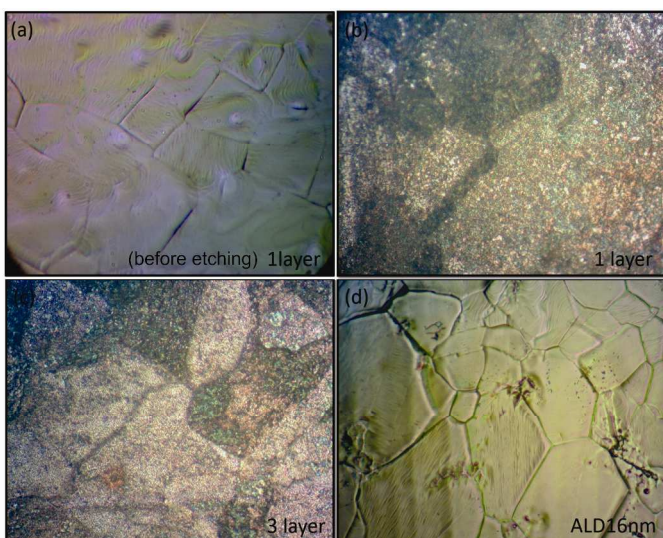


Figure S8. Comparison of changing Cu morphology by etching using different passivation methods(a) Cu/1LG before CV corrosion,(b-d) after CV corrosion: (b) Cu/1LG, (c) Cu/3LG, (d) Cu/1LG/16nm ALD

8. References

- (1) Hofmann, M.; Shin, Y.; Hsieh, Y.-P.; Dresselhaus, M.; Kong, J. A Facile Tool for the Characterization of Two-Dimensional Materials Grown by Chemical Vapor Deposition. *Nano Res.* **2012**, *5*, 504-511.
- (2) Tsen, A. W.; Brown, L.; Levendorf, M. P.; Ghahari, F.; Huang, P. Y.; Havener, R. W.; Ruiz-Vargas, C. S.; Muller, D. A.; Kim, P.; Park, J. Tailoring Electrical Transport across Grain Boundaries in Polycrystalline Graphene. *Science* **2012**, *336*, 1143-1146.
- (3) Hsieh, Y.-P.; Hofmann, M.; Kong, J. Promoter-Assisted Chemical Vapor Deposition of Graphene. *Carbon* **2013**, *67*, 417-423.
- (4) Dai, H. J.; Wang, X. R.; Tabakman, S. M. Atomic Layer Deposition of Metal Oxides on Pristine and Functionalized Graphene. *J. Am. Chem. Soc.* **2008**, *130*, 8152-8153.
- (5) Prasai, D.; Tuberquia, J. C.; Harl, R. R.; Jennings, G. K.; Bolotin, K. I. Graphene: Corrosion-Inhibiting Coating. *Acs Nano* **2012**, *6*, 1102-1108.
- (6) Ambrosi, A.; Bonanni, A.; Sofer, Z.; Pumera, M. Large-Scale Quantification of Cvd Graphene Surface Coverage. *Nanoscale* **2013**, *5*, 2379-2387.
- (7) Singh Raman, R. K.; Chakraborty Banerjee, P.; Lobo, D. E.; Gullapalli, H.; Sumandasa, M.; Kumar, A.; Choudhary, L.; Tkacz, R.; Ajayan, P. M.; Majumder, M. Protecting Copper from Electrochemical Degradation by Graphene Coating. *Carbon* **2012**, *50*, 4040-4045.